July, 2019

Surface plasmon induced enhancement in selective laser melting processes

Dentcho A. Genov, *Louisiana Tech University*
Raj K. Vinnakota, *Louisiana Tech University*

Surface plasmon induced enhancement in selective laser melting processes

Raj K. Vinnakota and Dentcho A. Genov
Department of Physics, Louisiana Tech University, Ruston, Louisiana, USA

Abstract

Purpose – Selective laser melting (SLM) is an advanced rapid prototyping or additive manufacturing technology that uses high power density laser to fabricate metal/alloy components with minimal geometric constraints. The SLM process is multi-physics in nature and its study requires development of complex simulation tools. The purpose of this paper is to study – for the first time, to the best of the authors' knowledge – the electromagnetic wave interactions and thermal processes in SLM based dense powder beds under the full-wave formalism and identify prospective metal powder bed particle distributions that can substantially improve the absorption rate, SLM volumetric deposition rate and thereby the overall build time.

Design/methodology/approach – We present a self-consistent thermo-optical model of the laser-matter interactions pertaining to SLM. The complex electromagnetic interactions and thermal effects in the dense metal powder beds are investigated by means of full-wave finite difference simulations. The model allows for accurate simulations of the excitation of gap, bulk and surface electromagnetic resonance modes, the energy transport across the particles, time dependent local permittivity variations under the incident laser intensity, and the thermal effects (joule heating) due to electromagnetic energy dissipation.

Findings – Localized gap and surface plasmon polariton resonance effects are identified as possible mechanisms toward improved absorption in small and medium size titanium powder beds. Furthermore, the observed near homogeneous temperature distributions across the metal powders indicates fast thermalization processes and allows for development of simple analytical models to describe the dynamics of the SLM process.

Originality/value – To the best of the authors' knowledge, for the first time the electromagnetic interactions and thermal processes with dense powder beds pertaining to SLM processes are investigated under full-wave formalism. Explicit description is provided for important SLM process parameters such as critical laser power density, saturation temperature and time to melt. Specific guidelines are presented for improved energy efficiency and optimization of the SLM process deposition rates.

Keywords Selective laser melting, Additive manufacturing, 3D printing, Metals, Surface plasmon, Cavity resonances, Radiation, Thermalization and deposition rate

Paper type Research paper

1. Introduction

Three-dimensional (3D) printing with metals and alloys using selective laser melting (SLM) is the most promising and successful additive manufacturing technique to date (Yap *et al.*, 2015; Eisenhut and Langefeld, 2013; Gibson *et al.*, 2010). The SLM is a layer-by-layer rapid manufacturing technology that uses high power laser beams to melt and fuse metallic powders in a controlled manner (Gibson *et al.*, 2010). The technology is known for printing high quality 3D metal-parts with high geometric complexity. A significant feature of the SLM is near-net shape production without the need for expensive molds or time consuming post-processing and high production flexibility (Thijs *et al.*, 2010; Garibaldi *et al.*, 2016). Owing to numerous advantages in comparison to traditional manufacturing technologies, the implementation of SLM in the industry has been rapidly increasing (Eisenhut and Langefeld, 2013; Wohlers Report, 2015; Pacurar and Pacurar, 2016; Mostafa *et al.*, 2017; Ventola, 2014). However, further improvements in productivity and reduction in costs are crucial factors that need to be addressed for future widespread SLM implementation.

In recent years, different methods have been proposed to address the above mentioned shortcoming. These include, use of higher power lasers to melt multiple layers at the same time (Bremen *et al.*, 2011), or use of multiple lasers (Buchbinder *et al.*, 2011). Increase in SLM productivity has been achieved by using up to four lasers simultaneously and by implementing the hull-core scanning strategy (dprinting, 2019). Unfortunately, limited installation space for optical components hinders further increase in the number of lasers. Moreover, the hull-core strategy mainly offers significant benefits to parts requiring heavy wall-thickness that are usually not manufactured using SLM. Hence, there is a clear need for alternative paths toward improved productivity. Currently, the SLM process is limited by the maximum laser energy deposited in the powder bed, which mainly depends on material properties (absorbance) as well as SLM process scan rates. Therefore, to improve productivity a comprehensive understanding of the complex laser-matter interactions with the powder bed is required.

The fundamental physics processes involved in SLM are complex and include scattering and absorption of laser

The current issue and full text archive of this journal is available on Emerald Insight at: **www.emeraldinsight.com/1355-2546.htm**

Rapid Prototyping Journal
25/6 (2019) 1135–1143

[ISSN 1355-2546]
[DOI 10.1108/RPJ-06-2018-0146]

Received 13 June 2018
Revised 4 May 2019
Accepted 6 May 2019

radiation into highly heterogeneous metal powders, heat transfer, formation of molten pools and its solidification, all within multiple length and time scales. Experimental and numerical approaches have been proposed to study these processes in metal powder materials (Tolochko *et al.*, 2000; Fischer *et al.*, 2003; Gusarov *et al.*, 2009; Boley *et al.*, 2016; Chan and Tien, 1974). The analysis of the absorption of electromagnetic energy from the laser is usually based on the solution of the corresponding diffraction problem under the ray approximation while the wave nature of the interactions, including excitation of cavity and especially surface resonances are commonly neglected (Baffou and Rigneault, 2011; Boley *et al.*, 2015; Gusarov and Kruth, 2005; Wang *et al.*, 2002; Argento and Bouvard, 1996). An alternative approach to geometrical optics method is proposed by utilizing Maxwell equations (Kovalev and Galjov, 2015). Optimization in the energy absorption by the metal powders could be possible by laser action on metal particles where laser pulse with frequency close to the particle's surface plasmon polariton (SPP) resonances are used, resulting in localized electron excitations, leading to optical resonance phenomena (Zayats *et al.*, 2005; Barnes *et al.*, 2003; Hutter and Fendler, 2004; Shinji and Takayuki, 2012). One of the most fascinating aspects of SPPs is the way light is channeled using the system geometries and has been used in wide range of application (Zhao *et al.*, 2006; Pendry, 2000; Zhang and Liu, 2008; Oulton *et al.*, 2009; Genov *et al.*, 2011; Vinnakota and Genov, 2014, 2017). Light-trapping layers using metallic plasmonic microstructures have gained significant attention (Linic *et al.*, 2011; Atwater and Polman, 2010; Schuller, 2010) and efficient resonant light absorption by several plasmonic nanostructures with microcavities (Long, 2009), and gap-plasmon resonators (Rand *et al.*, 2004; Moreau *et al.*, 2012) has been extensively studied. Regarding metal-based absorbers, absorption enhancement using stacked plasmonic resonators, colloidal microspheres and their corresponding arrays has been also presented (Hedayati, 2011; Wang *et al.*, 2015; Grandidier *et al.*, 2011; Kang, 2013; Liu, 2010). Extreme confinement and light trapping can convert the electromagnetic energy into heat with high efficiency and thus can fasten the initiation of the melting in SLM powders. Thus to study the complex electromagnetic and heat dissipation phenomenon in actual powder beds, where length scales can vary from nanometers into tens of micrometers, it is highly desirable to develop a general numerical and if possible high fidelity analytical models which can describe the system beyond the ray approximation and give accurate results for the powders volumetric temperature dependence on the laser beam parameters and metal particles sizes.

In this article we perform a comprehensive multi-physics study of the complex phenomena associated with light matter interactions in metal powder beds pertaining to SLM. A numerical framework is developed which self-consistently solves Maxwell's and heat equations to study the relevant electro and thermodynamic phenomenon. This model allows for accurate simulations of the excitation of gap, bulk and surface electromagnetic resonance modes, the energy transport across the powders, time dependent local permittivity variations at high powers and the thermal effects (joule heating) because of electromagnetic energy dissipation. We have acquired numerical data representing the local laser heating and temperature profiles for steady-state and transient illumination. The numerical results are compared with developed semi-analytical model showing an excellent agreement for powder beds consisting of titanium particles with sizes ranging from hundreds of nanometers up to tens of microns. The analytical model provides a qualitative and quantitative description of the volumetric temperature rise, critical laser power, saturation temperature and deposition rates as function of various optical and thermometric parameters. Finally, specific guidelines are outlined for potentially significant increase of the SLM energy efficiency and deposition rates.

2. Thermo-optical model

In a typical SLM process there are two competing mechanisms that are primarily responsible for the initiation of melting in the powder bed. The first mechanism is related to complex light matter interactions such as multiple reflections and scattering while the second is associated with heat re-distribution within the powder bed, thermal emission and conduction/convection heat transfer. To account for these strongly coupled effects a self-consistent thermo-optical model is developed. Full-wave finite difference (FD) calculations of the optical phenomena manifested within the powder bed are performed using the COMSOL electromagnetic module. The thermal effects due to Joule heating are accounted for by the COMSOL heat transfer module. A seamless integration between the two physical modules is accomplished by developing a MATLAB-based facilitator code. The code shares the inter-dependent physical parameters between the two separate modules and allows for self-consistent steady state and time dependent simulations.

Owing to multiple length and time scales involved in SLM, specific mesh size and time step constrains must be strictly enforced. The electromagnetic simulations are stable and sufficiently accurate as long as we set the mesh size $\Delta h = \delta/5$, where δ is the particles skin depth (the skin depth is generally much smaller than the wavelength λ at optical frequencies). For titanium, the skin depth is $\delta = 22$ nm (for $\lambda = 1.0\ \mu$m) (Lahiri *et al.*, 2010), and to accurately simulate the largest particle beds considered in this work (particle radius up to 10 microns) operational memory surpassing 30GB is required. Combined with adaptive meshing this memory constrain is easily addressed even on an average workstation. Hence, the historical use of ray tracing methods is no longer a necessity and the simulation community should transition to exact numerical calculations of the electromagnetic phenomenon associated with SLM. Such transition can provide a high fidelity codes that accurately capture new electromagnetic phenomenon such as excitation of surface electromagnetic states which are completely missed in commonly used ray approximation schemes. Apart from the spatial considerations the self-consistent thermo-optical model has to properly capture all relevant time scales as well. The numerical solutions of the heat equation are stable provided the time step is $\Delta t < \frac{1}{2\alpha_P}\ \Delta h^2 = \frac{1}{50\alpha_P}\delta^2 = 50$ps, where α_P is the particle thermal diffusivity (titanium is assumed in the estimate). This time step is sufficiently larger compared to the transient times in the electromagnetic simulations. As a result steady state solutions of the Maxwell's equations can be generated in each

time step, and the local Joule heating can be incorporated in the heat transfer module. This iterative process continues until saturation in the particle temperature or onset of melting is reached at macroscopic times.

2.1 Numerical simulations – isolated particle

To test the developed thermo-optical model we first consider a simple configuration comprising of a free standing titanium particle, see Figure 1(a). As we consider extreme thermodynamic conditions, actual temperature dependent thermo-physical parameters are considered in the model (Zhang *et al.*, 2013; Hatef and Meunier, 2015). As first step we consider steady state conditions where the absorption scattering cross-section obtained by the finite-difference model, shown in Figure 1(a), is found to match the Mie formalism (Bohren and Huffman, 1998). The particle absorption exhibits resonance behavior for small particles and asymptotically approaches the absorbance from a flat metal plane at large particles sizes. In Figure 1(b) we observe that while the local Joule heating can be highly inhomogeneous and localized within the particle skin depth, the corresponding steady-state temperature is near uniform. This is attributed to the fact that a homogenization of the temperature profile inside the particle is established rapidly and within a characteristic time $\tau \approx R^2/\alpha_P$, where R is the particle radius. For titanium particles with radius $R = 5\,\mu$m the corresponding characteristic time is $\tau \sim 2.7\,\mu$s.

To better understand the temporal dynamics of the particle heating process we have performed a set of time-dependent simulations shown in Figure 1(c) and (d). A linear increase of the volume averaged temperature with time is observed up until the onset of saturation due to thermal emission. In the simulations various conditions related to the particle sizes and input laser power densities are investigated. Figure 1(c) depicts the temperature rise and saturation for three separate laser power densities and titanium particle with fixed size $R = 0.5$ μm. The power densities are chosen such that we can separately investigate the three operational regimes where the saturation temperature is lower, equal and higher compared to the particle melting temperature T_m = 1,941 K (periodic-table, 2019). For laser power densities below the critical $P_0 < P_c = 320$ W/cm^2, the temperature saturates at maximum value lower than the particle melting temperature. At higher powers $P_0 > P_c$ the time to melt is inversely proportional to the power density and depends linearly on the particle size [see Figure 1(d)]. In all investigated cases and for laser power densities typical for SLM, the onset of melting or temperature saturation (for power densities less than the critical $P_0 < P_c$), happens within a few milliseconds. This time scale is much larger than the local temperature homogenization time τ which as we have showed above is within a few microseconds. The existence of two separate time scales pertaining to the SLM process allows for development of a simple analytical model which we present next.

Figure 1 (a) Absorption cross-section of isolated titanium (Ti) particle using the Mie theory. At the chosen operational wavelength $\lambda = 1.07$ μm (corresponding to Concept Laser Mlab cusing R 3D printer (concept-laser, 2019) the refractive index of titanium is $n_p = 3.474 + i4.0113$ (Johnson and Christy, 1974); (b) the local Joule heating is found to be predominantly along the polarization direction of the impinging radiation and the steady state temperature profile of the particle (R = 0.5 μm) irradiated with laser power density P_0 = 200 W/cm^2 is found to be remarkably homogeneous; (c), (d) the volume-averaged particle temperature as function of the elapsed time is obtained using the self-consistent multiphysics model (dots) and compared to the analytical result given by equation (2) (solid lines). In (c) the size of the particle is fixed at $R = 0.5$ μm and irradiated with three different laser power densities P_0 = (200,320,500) W/cm^2, while in (d) three different particle sizes are investigated at fixed laser power density P_0 = 500 W/cm^2. In the calculations the operational wavelength is set at 1.07 μm, and the particle melting temperature is shown with dashed line.

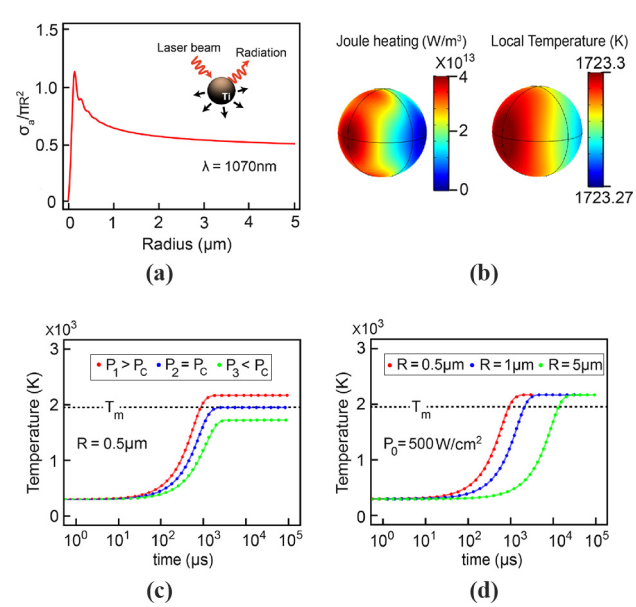

2.2 Analytical model

Starting with the local form of the heat equation, performing averaging over the particle volume and using the divergence theorem we arrive at:

$$\rho c_p V \frac{d\langle T(t)\rangle}{dt} = k_P \oint \vec{\nabla} T(\vec{r},t) \cdot d\vec{S} + \dot{Q} \tag{1}$$

where $\langle T(t)\rangle = V^{-1}\int T(\vec{r},t)dV$ is the volume average temperature, V is the particle volume, p is the particle mass density, c_P is the specific heat capacity, k_P is the thermal conductivity of the particle and $\dot{Q} = \sigma_a P_0$ is the Joule heating rate which depends on the incident laser power density P_0 and the absorption cross-section σ_a. The heat flux at the surface is because of conduction/convection and radiation losses and can be written as function of the average surface temperature $\langle T(t)\rangle_R = S^{-1}\int T(\vec{r},t)dS$ as follows:

$$\rho c_p V \frac{d\langle T(t)\rangle}{dt} = -hS\left(\langle T(t)\rangle_R - T_a\right) - \epsilon\sigma_B S\left(\langle T(t)\rangle_R^4 - T_a^4\right) + \dot{Q} \tag{2}$$

where $T_a = 300$ K is the ambient temperature, σ_B is the Boltzmann constant, and $\epsilon = \sigma_a/\pi R^2$ is the emissivity. For stagnant flow the heat transfer coefficient is given as $h = k_a/R$, where k_a is the thermal conductivity of the buffer gas. For times

sufficiently larger compared to the thermalization time $t \gg \tau$ but smaller compared to the time to melt (or saturation at lower powers) we can equal the average volumetric and surface temperatures $\langle T(t)\rangle = \langle T(t)\rangle_R = T(t)$. In this case Equation (2) has an exact analytical solution which however is rather cumbersome and not very illuminating. Instead, we recognize that SLM ambient conditions involve buffer gases with low thermal conductivities and high powder bed temperatures for which the conduction term can be neglected. The rate equation (2) then has a simple analytical solution in implicit form:

$$t = \frac{t_0}{2}\left(\tan^{-1}\left(\frac{T}{T_s}\right) + \tanh^{-1}\left(\frac{T}{T_s}\right) - \tan^{-1}\left(\frac{T_a}{T_s}\right) - \tanh^{-1}\left(\frac{T_a}{T_s}\right)\right) \quad (3)$$

where t is the time since the onset of heating, $t_0 = \frac{\rho c_p R}{3\epsilon\sigma_B T_s^3}$ is a characteristic time corresponding to reaching saturation, and $T_s = \left(T_a^4 + \frac{P_0}{4\sigma_B}\right)^{1/4}$ is the saturation temperature which is independent on the particle size. For a given melting temperature, T_m, the theory predicts a critical power density $P_c = 4\sigma_B\left(T_m^4 - T_a^4\right)$ required to initiate the melting process. For high powers such that $T_a \ll T_m \ll T_s$ a linear rise of temperature is expected $T \approx T_a + (t/t_0)T_s$, and the time to melt can be estimated as $t_m = \frac{t_0 T_m}{T_s} = \frac{4\rho c_p R T_m}{3\epsilon P_0}$, showing linear dependence with the particle size and inverse dependence on the incident power. This is consistent with the numerical findings in Figure 1(c, d), where we compare the analytical theory with the numerical results for different incident power densities and particle sizes. We observe an excellent agreement both in terms of predicting the transient behavior and steady state temperature. As discussed above, the analytical model is only applicable if a near homogeneous temperature is observed for macroscopic times or provided $t_m \gg \tau$. This condition sets a limit for the laser power density $P_0 < k_P T_m/R$, beyond which the analytical model cannot be trusted. For titanium particles with radius $R = 1\,\mu$m, the power densities must be lower than 4 MW/cm^2.

3. Dense metal powders

The developed thermo-optical models have been also extended to study the dense metal powders used in SLM. The system under consideration consists of a layer of closely packed (touching) titanium spheres resting on a substrate which represents the already melted pool and is depicted as an insert in Figure 2. In the numerical simulations, to account for the interactions of all particles within the powder layer, we consider a unit cell comprising of a single spherical titanium particle on top of a titanium substrate with periodic boundary conditions imposed across the system (in the plane parallel to the substrate). Imposing such periodic boundary conditions is a common approach used in the literature and is expected to capture the relevant physics in large systems (Großer *et al.*, 2012; Liu *et al.*, 2017; Panwisawas, 2017; Li, 2008). Also, in the COMSOL Heat Transfer Module the following heat transfer processes are included; conductive and convective heat transfer into the buffer gas, conductive transfer between

Figure 2 Absorptance vs particle size for closely packed (touching) titanium spheres arranged in square lattice on top of a titanium substrate (see insert). In the calculations the laser radiation is normal to the particle bed and the laser wavelength is set at 1.07 μm. Morphologically dependence resonances are manifested owing to electromagnetic interactions between neighbors and excitation of surface plasmon states (points A, B and C). In the figure we have also included the absorptance obtained from the ray-tracing method (dashed black line) which is independent on the particle radius (Gusarov and Kruth, 2005).

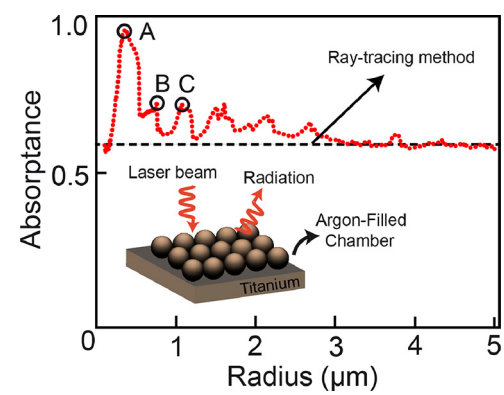

particles and substrate as well as black body radiation losses. The calculated absorptance under steady state conditions, normal laser incidence, fixed wavelength and varying particle sizes is shown in Figure 2.

Compared to a single non-interactive particle, see Figure 1(a), here we observe absorptance with added complexity. This added complexity is predominantly due of inter-particle field interactions that provide additional channels for excitation of morphology dependent resonances facilitated by surface plasmon polaritons (SPPs). The SPPs are transfer magnetic (TM) surface modes that propagate at the metal-dielectric interfaces. For planar surfaces the SPP wavevector is given as $k_{sp} = (\omega/c)\sqrt{\varepsilon_d\varepsilon_p/(\varepsilon_d + \varepsilon_p)}$, where ε_d and ε_p are dielectric and metal permitivities, respectively. For large metal particles and neglecting curvature effects the leading SPP resonances can be obtained using the standing-wave condition Re$[k_{sp} R] = 2n$, where $n = 1,2,\ldots$ For titanium particles illuminated with laser radiation at fixed free space wavelength $\lambda = 2\pi c/\omega = 1.07\,\mu$m, we obtain a set of resonance particle sizes $R = 0.34\ \mu$m, 0.68 μm, 1.02 μm,…. These correlate rather well with the absorptance peaks in Figure 2; manifested for $R = 0.37\ \mu$m (A point), $R = 0.75\ \mu$m (B point), and $R = 1.07\ \mu$m (C point). As the particle size increases, higher order SPP resonances are excited. The quality factor of these resonances generally decreases with the order and as a result gradual disappearing of the resonance structure is observed for large particles $R > 5\ \mu$m, with the absorbtance approaching $A \to 61.5$ per cent which is consistent with estimates using the ray tracing method (Gusarov and Kruth, 2005). Generally, in typical ray tracing codes surface resonance features such as excitation of surface plasmon polariton resonances are not captured. Using full-wave thermo-optical models, as the one described in this work, can effectively investigate the wave nature of interactions within the powder bed and capture the complex morphology dependent resonances (gap, bulk and surface electromagnetic resonances) that

concurrently have a significant effect on the absorptance. From Figure 2 we observe the absorptance reaching ~95.8 per cent for A point, ~73.5 per cent for B point and ~72.7 per cent for C point all values substantially larger than the absorptance predicted by the ray tracing method. Thus, using finer metal powders tuned to a particular morphology resonance can substantially improvise absorptance by up to 55 per cent (A point) as compared to course powders.

The numerically obtained steady-state electric field, joule heating and temperature distributions for titanium powders with particle sizes supporting SPP resonances are depicted in Figure 3. Close inspection of the local electric field profiles provides further validation of the proposed explanation of the resonance effects as facilitated by SPP standing-waves; see Figure 3(a-f). While the local electric field and corresponding Joule heating are aligned with the laser polarization direction and show highly inhomogeneous profiles, the steady-state surface temperature is remarkably homogeneous [Figure 3 (g-i)]. As discussed in the preceding sections, this is because of fast thermalization times sufficiently larger than the homogenization time $t \gg \tau = R^2/\alpha_P$. This fact, similarly to the case of a free standing particle, allows the implementation of the analytical model Equation (3) with few simple modifications. To account for the change in geometry (dense powders) in the model the Joule heating rate is now given by $\dot{Q} = AP_0S$, the emissivity is equal to the absorptance $\epsilon = A$ and $S = 4R^2$ is the cross-sectional area of the unit cell (touching spheres).

The temporal response of the volume averaged particle temperature calculated using the numerical method and analytical theory is shown in Figure 4. In the calculations we consider again a set of input power densities and particle sizes chosen to exemplify the various regimes of operation. Figure 4(a) depicts the temperature versus time for periodic array of 0.35 μm sized particles (matching the $n = 1$ SPP resonance) at input powers below, at and above critical. Similar behavior to that of a free standing particle is observed. The main difference compared to free standing particle is that for dense powders the critical laser power density is reduced by a factor of $\approx 1/4$. This is consistent with the shading effect owing to the adjacent particles which can reabsorb the thermal radiation if the angle of emission is $\theta > \theta_M$. For closely packed powders the angle of the radiation window is $\theta_M = \tan^{-1}(2)$ and the critical power is reduced by a factor proportional to the radiation solid angle fraction $\Omega_R/4\pi = \frac{1}{2}\int_0^{\theta_M} \sin(\theta)d\theta = 0.27 \approx 1/4$. In all three cases the analytical theory closely matches the numerical results and melting conditions are reached within a few milliseconds. Similar consistency is observed at fixed incident power density and varying particle sizes, shown in Figure 4(b). In the linear regime, the time to melt $t_m = \frac{\pi \rho c_p R T_m}{3AP_0}$ is proportional to the particle radius which is clearly evident in the presented data. Note, in the presentation we use log-normal plots to capture the behavior for large range of times.

Figure 3 (a), (b), (c) local electric field profiles because of impinging (from the left) laser radiation showing excitation of standing surface waves associated with surface plasmon polaritons (SPPs); (d), (e), (f) the SPP modes induce localized Joule heating which is found to be predominantly on the polarization direction of the impinging radiation; (g), (h), (i) the local steady state temperature on the particle surface shows a highly homogenous distribution despite the strongly localized Joule heating. In the calculations, the operational wavelength is set at 1.07 μm and the incoming laser beam power density is $P_0 = 40$ W/cm^2.

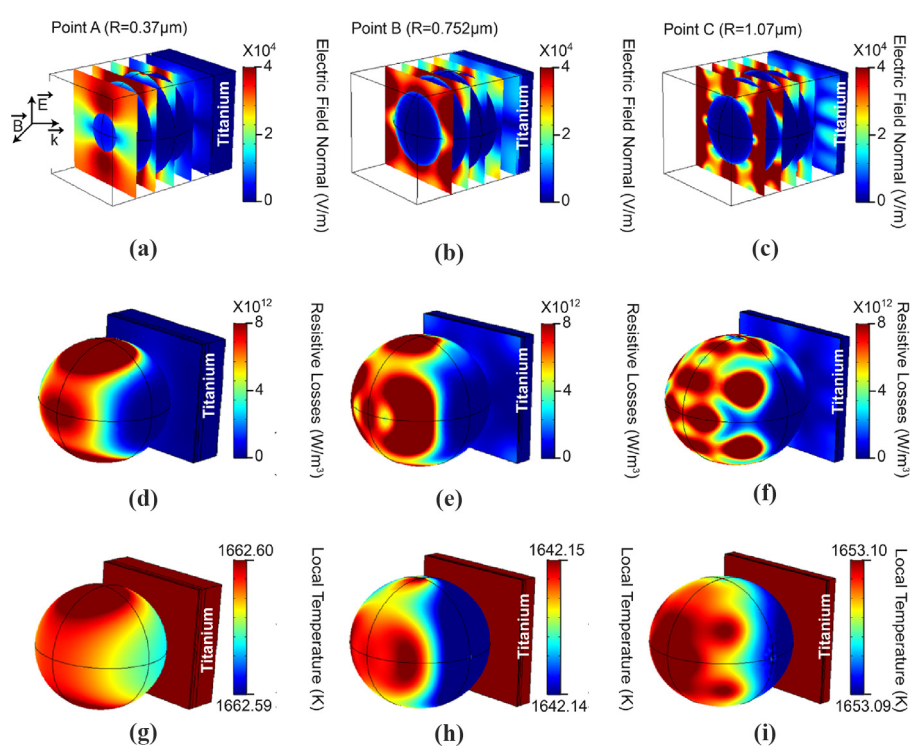

Figure 4 The volume-averaged particle temperature as function of the elapsed time for periodic array of titanium particles obtained using the self-consistent multiphysics model (dots) and compared to the analytical result (solid line). (a) The size of the particle is set to match the n = 1 SPP resonance (point A) and is irradiated with three different laser power densities P_0 = (40,82,200) W/cm^2; (b) the temperature vs time calculated for periodic arrays of titanium particles with varying sizes and irradiated with a constant laser power density P_0 = 200 W/cm^2. In the calculations the operational wavelength is set at 1.07 μm.

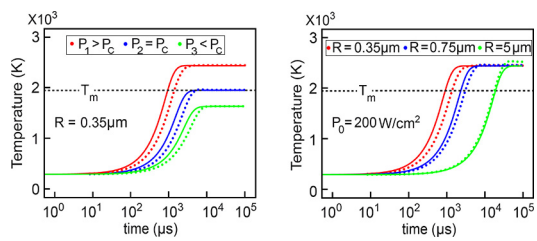

The presented study provides an insight into the intra- and inter-particle heat transfer processes within the powder bed. Inter-particle heat transfer is typically governed by conduction into the buffer gas (argon in our case), contact conduction between the particles and to the substrate they reside on. For typical SLM buffer gasses and low pressures the conductive transfer is weaker compared to radiation losses and can be neglected for power densities $P_0 < k_P T_m/R$. When considering the intra-particle heat transfer, the time scale defining the transient processes are typically much smaller than the time scales governing particle melting. In other words, under typical SLM conditions, conductive homogenization of non-uniform energy and temperature distributions across the powder bed and inside the individual particles happen extremely fast and we can safely consider the metal powder under near uniform temperature at macroscopic times.

4. Selective laser melting – volumetric deposition rate and energy efficiency

Some of the major obstacles for the widespread implementation of metal printing based on SLM is the time-consuming processing which can take hours to create a single component. Increasing the printing rate and improving the energy efficiency are main goals for the industry. To access possible strategies for such technology improvements we have performed a systematic study of the volumetric deposition rate versus average particle size and input laser power density. The deposition rate is estimated as $\dot{V} = 4\pi R^3 N/3t_m = \pi R W_0/3P_0 t_m$, where $N = S_0/4R^2$ is the number of particles within the laser beam spot area S_0, $W_0 = S_0 P_0$ is the incident laser beam power, and $t_m = t_m(A, P_0, R)$ is the melting onset time which is a function of the absorptance A, power density P_0 and average particle size. In Figure 5(a) we present the volumetric deposition rates for various laser power densities and closely packed titanium spheres arranged in square lattice. In the calculations we have fixed the total laser power at W_0 = 100 W, typical for SLM printing machines (concept-laser, 2019; Imprimalia, 2019). A substantial speed up could be achieved for powder beds with mean particles sizes that support excitation of SPP resonances and hence increased absorptance. Increasing the laser power density or decreasing the laser spot size lead to overall increase in deposition until it reaches a fundamental limit which we refer to as a maximum volumetric deposition rate (MVDR). This limit can be obtained from the rate equation (3), which is solved in the limit of high powers, rapid temperature rise and negligible radiation losses. Under these conditions the time to melt is $\tilde{t}_m = \rho c_p V(T_m - T_a)/4AR^2 P_0$ and the maximum volumetric deposition rate is $\dot{V}_{MVDR} = AW_0/[\rho c_p(T_m - T_a)]$, independent of the laser power density.

In actual dense powder beds, there is always some finite spreading in the particle sizes. To simulate such a system we consider a sample of tightly packed powder beds with particle sizes distributed according to a skewed-normal probability distribution function $g(R'; R, \sigma) = R' \exp\left(-\left(\frac{R'-R}{\sigma(R)}\right)^2\right)$. This distribution is chosen instead of normal distribution, as it better represents the experiments (Sudbrack *et al.*, 2018; Baitimerov *et al.*, 2018; Zegzulka *et al.*, 2018; Shuai, 2018; Andrade *et al.*, 2017; Zhang and Coddet, 2015; Dong *et al.*, 2018) and has a physically meaningful limit for $R' \to 0$. The average absorption of the powders is then calculated as:

$$\langle A \rangle_{(R,\sigma)} = \frac{\int_0^\infty A(R') g(R'; R, \sigma) dR'}{\int_0^\infty g(R'; R, \sigma) dR'} \tag{4}$$

Figure 5 Volumetric deposition rate as a function of particle size and incident laser intensity for (a) closely packed titanium spheres arranged in square lattice and (b), (c) random arrangement of closely packed titanium spheres with two statistical spread-outs σ_0 = (0.05,0.2); and (d) efficiency as a function of incident laser intensity. In the calculations the operational wavelength is set at 1.07 μm, incident laser power as W_0 = 100 W. The corresponding maximum volumetric deposition rate (MVDR) is depicted by black dots.

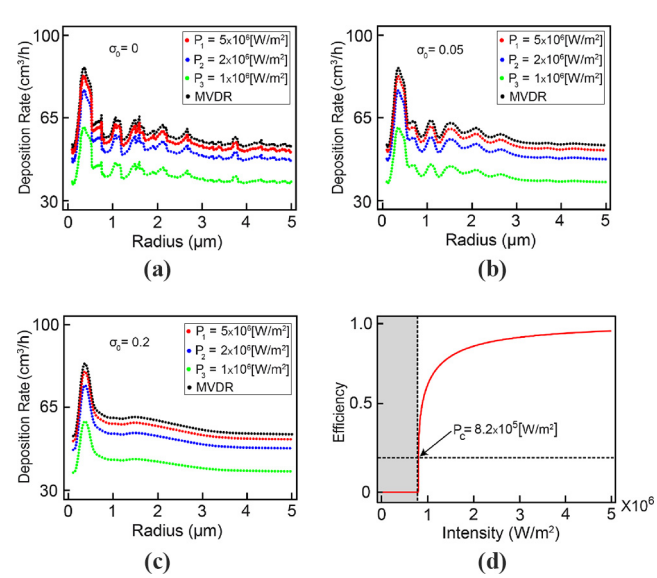

where $A(R')$ is the numerically obtained absorptance of the closely packed (touching) titanium spheres as per Figure 2. In the model we also assume a statistical spreading proportional to the mean radius $\sigma(R) = \sigma_0 R$, which correlates to the experimental findings (Sudbrack *et al.*, 2018; Baitimerov *et al.*, 2018; Zegzulka *et al.*, 2018; Shuai, 2018; Andrade *et al.*, 2017; Zhang and Coddet, 2015; Dong *et al.*, 2018). Finally, equation (4) is used to estimate the melting onset time $t_m = t_m(\langle A \rangle_{(R,\ \sigma)}, P_0, R)$ and volumetric deposition rate $\dot{V}$. Our results are shown in Figures 5(b, c). Generally, we observe that individual resonances are preserved for moderate spreading of the particle sizes, while the higher order resonances are completely "averaged away" for highly dispersed powders with $\sigma_0 \geq 0.2$. Despite the averaging effects the general trend of increasing deposition rate with decreasing particle size is preserved.

Apart from increasing the speed of the printing process it is also important to study the SLM energy efficiency. The efficiency can be defined as the fraction $\eta = U_p/U_L$ of the particle thermal energy $U_p = \rho c_p V(T_m - T_a)$ to the laser energy $U_L = \dot{Q} t_m$ deposited up to the onset of melting. The efficiency can also be written as the ratio between the times to melt with and without radiation losses, $\eta = \tilde{t}_m/t_m$, and is depicted in Figure 5(b). The efficiency has a strong dependency on the incident laser powder density, and goes to zero at the critical power. Interestingly, it is also found to be independent of the particle size and absorption. This is because U_L and U_p are both proportional to the particle volume and in the case of energy losses owing to radiation only the thermal emissivity is simply proportional to the absorption, which leads to saturation temperature independent on the absorbance and particle size. However, at intermediate and high buffer gas pressures the conductive heat transfer into the gas will start to play a more significant role. In this case the efficiency is sensitive to the powder bed particle size distribution. Overall, under typical SLM condition it can be concluded that using smaller laser focus spot sizes, optimal powder density along with particle/grain sizes that support plasmonic resonances may substantially improve deposition rates and energy efficiency. Because optimization is achieved for particle size distributions tailored to the excitation of surface plasmon resonances this points toward the need to develop powder beds consisting of particle sizes smaller than those currently used by the industry. Such shift toward finer powder beds can also lead to higher morphological uniformity of the melt pools and hence improved metallurgical microstructure of the printed parts, finer geometrical resolutions along with improved surface quality. However, it must be also recognized that using finer powder beds can also lead to issues related to clean up, contamination and layers deposition. If these technical issues are resolved there is a clear path toward further improvements in the SLM technology.

5. Conclusion

In summary we have developed a self-consistent thermo-optical model of the laser interactions with dense metal powder beds related to the SLM processes and studied the relevant electromagnetic and thermodynamic phenomenon. For this we have introduced a coupled finite difference time domain (FDTD) computational model which simultaneously solves the Maxwell's and the heat transfer equations. The model used adaptive meshing and can be executed in parallel. This allows full-wave calculations of spatial domains sufficiently large to model the SLM processes without use of approximated methods such as ray tracing. The presented approach is easy to implement and provides a new direction for the simulation community for transition into exact numerical simulations associated with SLM. Using the developed numerical method we have performed extensive studies of the local laser heating and temperature profiles for steady-state and transient illumination. It is observed that under typical SLM conditions the deposited laser energy is thermalized within a time scale substantially shorter compared to the time to melt, leading to highly homogeneous temperature profiled across the powder beds. This allows the implementation of a simple analytical model to provide a qualitative and quantitative description of the volumetric temperature rise in the powder beds as a function of the various optical and thermometric parameters. Overall, our results show that metal powder beds comprising particle size distributions supporting surface plasmon polariton (SPP) resonances can greatly improves the absorption rate and hence the SLM volumetric deposition rate.

References

Andrade, A.B., Ferreira, N.S. and Valerio, M.E.G. (2017), "Particle size effects on structural and optical properties of BaF 2 nanoparticles", *RSC Advances*, Vol. 7 No. 43, pp. 26839-26848.

Argento, C. and Bouvard, D. (1996), "A ray tracing method for evaluating the radiative heat transfer in porous media", *International Journal of Heat and Mass Transfer*, Vol. 39 No. 15, pp. 3175-3180.

Atwater, H.A. and Polman, A. (2010), "Plasmonics for improved photovoltaic devices", *Nature Materials*, Vol. 9 No. 3, pp. 205-213.

Baffou, G. and Rigneault, H. (2011), "Femtosecond-pulsed optical heating of gold nanoparticles", *Physical Review B*, Vol. 84, p. 35415.

Baitimerov, R., Lykov, P., Zherebtsov, D., Radionova, L., Shultc, A. and Prashanth, K.G. (2018), "Influence of powder characteristics on processability of AlSi12 alloy fabricated by selective laser melting", *Materials (Basel)*, Vol. 11 No. 5.

Barnes, W.L., Dereux, A. and Ebbesen, T.W. (2003), "Surface plasmon subwavelength optics", *Nature*, Vol. 424 No. 6950, pp. 824-830.

Bohren, C.F. and Huffman, D.R. (1998), *Absorption and Scattering of Light by Small Particles*, Wiley-VCH Verlag GmbH, Weinheim.

Boley, C.D., Khairallah, S.A. and Rubenchik, A.M. (2015), "Calculation of laser absorption by metal powders in additive manufacturing", *Applied Optics*, Vol. 54 No. 9, p. 2477.

Boley, C.D., Mitchell, S.C., Rubenchik, A.M. and Wu, S.S.Q. (2016), "Metal powder absorptivity: modeling and experiment", *Applied Optics*, Vol. 55 No. 23, pp. 6496-6500.

Bremen, S., Buchbinder, D., Meiners, W. and Wissenbach, K. (2011), "Mit selective laser melting auf dem weg zur serienproduktion?", *Laser Technik Journal*, Vol. 8 No. 6, pp. 271-278.

Buchbinder, D., Schleifenbaum, H., Heidrich, S., Meiners, W. and Bültmann, J. (2011), "High power selective laser melting (HP SLM) of aluminium parts", *Physics Procedia*, Vol. 12, pp. 271-278.

Chan, C.K. and Tien, C.L. (1974), "Radiative transfer in packed spheres", *Journal of Heat Transfer*, Vol. 96 No. 1, pp. 52-58.

Concept-laser (2019), available at: www.concept-laser.de/en/products/machines/mlab-cusing.html

Dong, Z., Zhang, X., Shi, W., Zhou, H., Lei, H. and Liang, J. (2018), "Study of size effect on microstructure and mechanical properties of AlSi10Mg samples made by selective laser melting", *Materials*, Vol. 11 No. 12, p. 2463.

Dprinting (2019), available at: https://3dprinting.co.uk/news/hull-core-building-strategy/

Eisenhut, M. and Langefeld, B. (2013), *Additive Manufacturing: A Game Changer for the Manufacturing Industry*, Roland Berger Strategy Consultants GmbH, Munich.

Fischer, P., Romano, V., Weber, H.P., Karapatis, N.P., Boillat, E. and Glardon, R. (2003), "Sintering of commercially pure titanium powder with a Nd: yAG laser source", *Acta Materialia*, Vol. 51 No. 6, p. 1651.

Garibaldi, M., Ashcroft, I., Simonelli, M. and Hague, R. (2016), "Metallurgy of high-silicon steel parts produced using selective laser melting", *Acta Materialia*, Vol. 110, pp. 207-216.

Genov, D.A., Oulton, R.F., Bartal, G. and Zhang, X. (2011), "Anomalous spectral scaling of light emission rates in low-dimensional metallic nanostructures", *Physical Review B*, Vol. 83, p. 245312.

Gibson, I., Rosen, D.W. and Stucker, B. (2010), *Additive Manufacturing Technologies*, Springer, p. 238.

Grandidier, J., Callahan, D.M., Munday, J.N. and Atwater, H. A. (2011), "Light absorption enhancement in thin-film solar cells using whispering gallery modes in dielectric nanospheres", *Advanced Materials*, Vol. 23 No. 10, pp. 1272-1276.

Großer, J., Furstenberg, R., Kendziora, C.A., Papantonakis, M.R., Borchert, J. and Andrew McGill, R. (2012), "Modeling of the heat transfer in laser-heated small particles on surfaces", *International Journal of Heat and Mass Transfer*, Vol. 55 Nos 25/26, pp. 8038-8050.

Gusarov, A.V. and Kruth, J.-P. (2005), "Modelling of radiation transfer in metallic powders at laser treatment", *International Journal of Heat and Mass Transfer*, Vol. 48 No. 16, p. 3423.

Gusarov, A.V., Yadroitsev, I., Bertrand, P. and Smurov, I. (2009), "Model of radiation and heat transfer in laser-powder interaction zone at selective laser melting", *Journal of Heat Transfer*, Vol. 131 No. 7, p. 072101.

Hatef, A. and Meunier, M. (2015), "Plasma-mediated photothermal effects in ultrafast laser irradiation of gold nanoparticle dimers in water", *Optics Express*, Vol. 23 No. 3, pp. 1967-1980.

Hedayati, M.K. (2011), "Design of a perfect black absorber at visible frequencies using plasmonic metamaterials", *Advanced Materials*, Vol. 23 No. 45, pp. 5410-5414.

Hutter, E. and Fendler, J.H. (2004), "Exploitation of localized surface Plasmon resonance", *Advanced Materials*, Vol. 16 No. 19, pp. 1685-1706.

Imprimalia (2019), available at: http://imprimalia3d.com/services/slm-50

Johnson, P.B. and Christy, R.W. (1974), "Optical constants of transition metals: ti, V, Cr, Mn, Fe, Co, Ni, and Pd", *Physical Review B*, Vol. 9 No. 12, pp. 5056-5070.

Kang, G. (2013), "Broadband Light-Trapping enhancement in an ultrathin film a-Si absorber using whispering gallery modes and guided wave modes with dielectric Surface-Textured structures", *Advanced Materials*, Vol. 25 No. 18, pp. 2617-2623.

Kovalev, B. and Galjov, R.V. (2015), "The application of Maxwell's equations for numerical simulation of processes during laser treatment of materials", *Journal of Physics D: Applied Physics*, Vol. 48 No. 30, p. 305501.

Lahiri, B., Dylewicz, R., De La Rue, R.M. and Johnson, N.P. (2010), "Impact of titanium adhesion layers on the response of arrays of metallic split-ring resonators (SRRs)", *Optics Express*, Vol. 18 No. 11, p. 11202.

Li, S. (2008), "Boundary conditions for unit cells from periodic microstructures and their implications", *Composites Science and Technology*, Vol. 68 No. 9, pp. 1962-1974.

Linic, S., Christopher, P. and Ingram, D.B. (2011), "Plasmonic-metal nanostructures for efficient conversion of solar to chemical energy", *Nature Materials*, Vol. 10 No. 12, pp. 911-921.

Liu, Z. (2017), "Ultra-broadband tunable resonant light trapping in a two-dimensional randomly microstructured plasmonic-photonic absorber", *Scientific Reports*, Vol. 7, p. 43803.

Liu, Z., Zhan, P., Chen, J., Tang, C., Yan, Z., Chen, Z. and Wang, Z. (2010), "Dual broadband near-infrared perfect absorber based on a hybrid plasmonic-photonic microstructure", *Optics Express*, Vol. 21 No. 3, p. 3021.

Long, Y.B. (2009), "Improving optical performance of inverted organic solar cells by microcavity effect", *Applied Physics Letters*, Vol. 95, p. 193301.

Moreau, A. (2012), "Controlled-reflectance surfaces with film-coupled colloidal nanoantennas", *Nature*, Vol. 492 No. 7427, pp. 86-89.

Mostafa, A., Rubio, I.P., Brailovski, V., Jahazi, M. and Medraj, M. (2017), "Structure, texture and phases in 3D printed IN718 alloy subjected to homogenization and HIP treatments", *Metals*, Vol. 7 No. 6.

Oulton, R.F. (2009), "Plasmon lasers at deep subwavelength scale", *Nature*, Vol. 461 No. 7264, pp. 629-632.

Pacurar, R. and Pacurar, A. (2016), *Applications of the Selective Laser Melting Technology in the Industrial and Medical Fields. In New Trends in 3D Printing*, in Shishkovsky, I.V. (Ed.), INTECH, Rijeka.

Panwisawas, C. (2017), "Mesoscale modelling of selective laser melting: thermal fluid dynamics and microstructural evolution", *Computational Materials Science*, Vol. 126, pp. 479-490.

Pendry, J.B. (2000), "Negative refraction makes a perfect lens", *Physical Review Letters*, Vol. 85 No. 18, pp. 3966-3969.

periodic-table (2019), available at: www.rsc.org/periodic-table/element/22/titanium

Rand, B.P., Peumans, P. and Forrest, S.R. (2004), "Long-range absorption enhancement in organic tandem thin-film solar cells containing silver nanoclusters", *Journal of Applied Physics*, Vol. 96 No. 12, pp. 7519-7526.

Schuller, J.A. (2010), "Plasmonics for extreme light concentration and manipulation", *Nature Materials*, Vol. 9 No. 3, pp. 193-204.

Shinji, H. and Takayuki, O. (2012), "Plasmonics: visit the past to know the future", *Journal of Physics D: Applied Physics*, Vol. 45, p. 433001.

Shuai, C. (2018), "Lanthanum-Containing magnesium alloy with antitumor function based on increased reactive oxygen species", *Applied Sciences*, Vol. 8 No. 11, p. 2109.

Sudbrack, C.K. (2018), "Impact of powder variability on the microstructure and mechanical behavior of selective laser melted alloy 718", *Proceedings of the 9th International Symposium on Superalloy 718 & Derivatives: Energy, Aerospace, and Industrial Applications*, pp. 89-113.

Thijs, L., Verhaeghe, F., Craeghs, T., Humbeeck, J.V. and Kruth, J.P. (2010), "A study of the microstructural evolution during selective laser melting of Ti-6Al-4V", *ActaMaterialia*, Vol. 58 No. 9, pp. 3303-3312.

Tolochko, N.K., Khlopkov, Y.V., Mozzharov, S.E., Ignatiev, M.B., Laoui, T. and Titov, V.I. (2000), "Absorptance of powder materials suitable for laser sintering", *Rapid Prototyping Journal*, Vol. 6 No. 3, p. 155.

Ventola, C.L. (2014), "Medical applications for 3D printing: current and projected uses", *P T*, Vol. 39 No. 10, pp. 704-711.

Vinnakota, R.K. and Genov, D.A. (2014), "Terahertz optoelectronics with surface Plasmon polariton diode", *Scientific Reports*, Vol. 4, pp. 20-27.

Vinnakota, R.K. and Genov, D.A. (2017), "Active control of charge density waves at degenerate semiconductor interfaces", *Scientific Reports*, Vol. 7, pp. 10778.

Wang, D., Zhu, W., Best, D., Camden, J.P. and Crozier, K.B. (2015), "Wafer-scale metasurface for total power absorption, local field enhancement and single molecule Raman spectroscopy", *Scientific Reports*, Vol. 3, p. 2867.

Wang, X.C., Laoui, T., Bonse, J., Kruth, J.P., Lauwers, B. and Froyen, L. (2002), "Direct selective laser sintering of hard metal powders: experimental study and simulation", *The International Journal of Advanced Manufacturing Technology*, Vol. 19 No. 5, p. 351.

Wohlers Report (2015), "3D printing and additive manufacturing state of the industry", Annual Worldwide Progress Report, Wohlers Associates.

Yap, C.Y., Chua, C.K., Dong, Z.L., Liu, Z.H., Zhang, D.Q., Loh, L.E. and Sing, S.L. (2015), "Review of selective laser melting: materials and applications", *Applied Physics Reviews*, Vol. 2 No. 4, p. 41101.

Zayats, A.V., Smolyaninov, A.A., II. and Maradudin, (2005), "Nano-optics of surface Plasmon polaritons", *Physics Reports*, Vol. 408 Nos 3/4, pp. 131-314.

Zegzulka, J., Gelnar, D., Jezerska, L., Ramirez-Gomez, A., Necas, J. and Rozbroj, J. (2018), "Internal friction angle of metal powders", *Metals*, Vol. 8 No. 4, p. 255.

Zhang, B. and Coddet, C. (2015), "Selective laser melting of iron powder: observation of melting mechanism and densification behavior via Point-Track-Surface-Part research", *Journal of Manufacturing Science and Engineering*, Vol. 138 No. 5, pp. 51001-51009.

Zhang, W., Li, Q. and Qiu, M. (2013), "A plasmon ruler based on nanoscale photothermal effect", *Optics Express*, Vol. 21 No. 1, pp. 172-181.

Zhang, X. and Liu, Z. (2008), "Superlenses to overcome the diffraction limit", *Nature Materials*, Vol. 7 No. 6, pp. 435-441.

Zhao, J., Zhang, X., Yonzon, C.R., Haes, A.J. and Van Duyne, R.P. (2006), "Localized surface plasmon resonance biosensors", *Nanomedicine*, Vol. 1 No. 2, pp. 219-228.

Corresponding author

Dentcho A. Genov can be contacted at: dgenov@latech.edu